Preparation and Analysis of Activated Carbon Derived from Yellowfin Tuna Fishbone using a Straightforward Carbonization Technique

Zuriah Sitorus (✉), Kurnia Sembiring, Emita Sembiring, Enda Rasilta Tarigan, and Doli Bonardo

University of Sumatera Utara, Medan, 20155, Indonesia
zuriah@usu.ac.id

Abstract. A successful preliminary study was conducted to examine the characteristics of activated carbon derived from yellowfin tuna fishbone using the carbonization method due to its ease and efficiency. Surface morphology and elemental composition analysis of activated carbon was performed using SEM-EDX, while XRD techniques were used to determine crystalline properties and the impact of carbonization temperature on material properties. The study findings indicated a strong correlation between carbonization temperature and the morphology and crystallinity of activated carbon. The surface morphology of carbon samples carbonized at 600 °C had higher impurity concentration compared to those synthesized at 700 °C and 800 °C. However, increasing the temperature resulted in a rougher surface formation. The XRD analysis revealed that an increase in carbonization temperature up to 800 °C contributed to higher carbon crystallinity due to better alignment of carbon chains, leading to a reduction in spacing between planes and the removal of disorganized carbon.

Keywords: Activated Carbon, Yellowfin Tuna Fishbone, Straightforward Carbonization Technique

1 Introduction

Activated carbon is a widely used and effective adsorbent in water treatment processes, owing to its high surface area and porous structure. Carbon-hydroxyapatite, a carbon-based material produced by heating materials containing carbon and calcium at high temperatures, has emerged as an alternative adsorbent that offers superior adsorption power and surface area compared to other adsorbents, including activated carbon [1]–[5]. Raw materials for this process include charcoal from various sources, such as animals, plants, waste, or minerals, that contain carbon [6], [7].

To generate carbon, a carbon source material undergoes thermal decomposition, also known as carbonation. This process begins with dehydration to remove water from the raw material [8]. Next, the organic matter breaks down into carbon elements in the form of charcoal through the process of carbonization in an oxygen-free environment without

M. Setiyo et al. (eds.), *Proceedings of the 4th Borobudur International Symposium on Science and Technology 2022 (BIS-STE 2022)*, Advances in Engineering Research 225,
https://doi.org/10.2991/978-94-6463-284-2_34

the use of chemicals [9], [10]. The large amount of human consumption waste has attracted researchers to increase research that utilizes this waste as an adsorbent source to reduce environmental pollution [11].

Heating animal bone waste at high temperatures not only generates carbon but also hydroxyapatite components, which consist of calcium, phosphate, and oxygen [12], [13]. The presence of hydroxyapatite is evident in the XRD results showing a crystal pattern [14]. As the combustion temperature rises, the carbon content decreases, and the powder turns white, indicating the formation of calcium [15]. This is due to the conversion of the organic component, carbon, into the primary inorganic component of bones, which is calcium.

Yellowfin tuna, a highly valued fish, is typically found in the upper layers of ocean waters [16]. It is a popular fish in Indonesian seas and commands a high selling price. However, only the flesh of the fish is typically used to make canned tuna meat, resulting in roughly 50% - 60% of the fish being discarded as waste. Tuna fish bones, which make up a significant portion of this waste, pose a major environmental pollution concern due to their large size [17]. In this study, we synthesized activated carbon from yellowfin tuna fishbone using a carbonization technique and analyzed the effect of carbonization temperature on the crystalline properties and surface morphology.

The novelty of this study lies in the use of yellowfin tuna fishbone as a raw material for the production of activated carbon through the carbonization process. This approach addresses the issue of waste management while also producing a valuable adsorbent. Furthermore, the impact of different carbonization temperatures on the crystalline properties and surface morphology of the resulting activated carbon from tuna fishbone is investigated, providing insight into the optimal conditions for producing high-quality adsorbent materials from this waste source. This study presents a potential solution to the growing environmental pollution problem caused by the large amounts of waste generated by the tuna industry.

2 Method

Initially, the waste tuna bones are cleansed to remove dirt, such as soil, leaves, and other debris that adheres to the remaining tuna meat. Afterward, the bones are boiled at 50 °C for an hour to soften any residual meat. Subsequently, the bones are sectioned at the joints to extract surplus fat from the tuna marrow. Following this, the bones are sun-dried for a week until they become brittle. The resulting fish bone powder is pulverized with a hammer and hard mill blender. This powder is then heated at 110 °C for 10 hours, yielding activated carbon with a dark black hue, apart from the samples carbonized at 800°C, which possess a slightly greyish tint, as indicated in Fig. 1. Additionally, the fish bone powder undergoes carbonization in a muffle furnace at 300, 400, and 500 °C for an hour, creating activated carbon samples labeled C300, C400, and C500, respectively. Lastly, the carbon powder is passed through an 80 Mesh sieve.

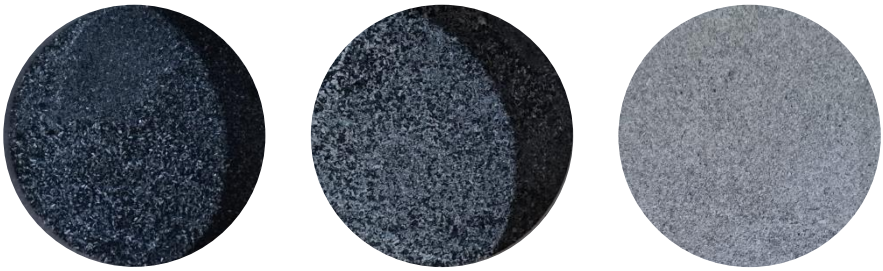

Fig. 1. The carbonized sample of C600 (a), C700 (b), and C800 (c).

3 Results and Discussion

3.1 X-Ray Diffraction (XRD)

XRD testing was performed on all samples to identify their crystal structure, and the Match application was used to determine the crystal size. Fig. 2 displays the diffraction patterns of carbon samples that were burned at different temperatures of 600, 700, and 800 °C. Although the three samples showed mostly similar diffraction patterns, there were minor differences in the intensity of some peaks. Overall, the three carbon samples produced from tuna bones exhibited an amorphous structure with crystalline peaks attributed to the hydroxyapatite crystalline phase (JCPDS PDF# 09-0432). The diffraction peak at 2theta 25.95° in the C600 sample showed a low intensity, which increased by approximately 90% in the C700 sample. However, the intensity of this peak decreased in the C800 sample by approximately 92%. Increasing the carbonization temperature can decrease the quality of crystallization when it reaches a steady temperature limit. However, this does not apply to other peaks that had increased intensity as the carbonization temperature reached 800 °C. The diffraction peak at 2theta 33.52° showed a significant increase in intensity in the C800 sample, surpassing the intensity value at the diffraction peak at 2theta 31.63°. This suggests that carbonization temperature is highly effective in enhancing the crystalline properties of activated carbon [18], [19].

The XRD data is a useful tool for analyzing the structural properties of materials, particularly their crystal structures. However, it is important to note that XRD data only provides information on the crystalline phase of the material, and not on its amorphous content. In addition, the peak broadening observed in the XRD data may also reflect the degree of crystalline order in the sample [20]. Therefore, it is important to use complementary techniques such as Raman spectroscopy or transmission electron microscopy to obtain a more complete understanding of the crystal structure of the materials. Nonetheless, the results from this study provide valuable insights into the effect of carbonization temperature on the crystalline properties of activated carbon derived from tuna bones, which can be useful for the optimization of the production process and the design of new materials with tailored properties.

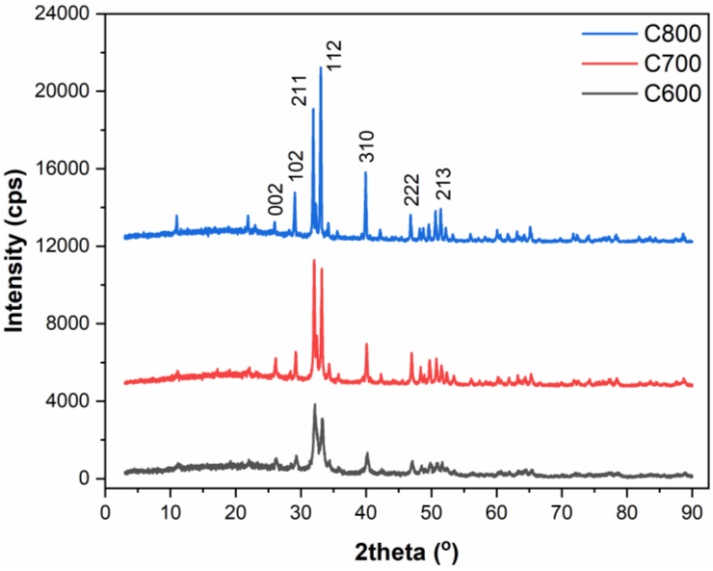

Fig. 2. XRD pattern of C600, C700, and C800 samples

Characterization by XRD showed that the resulting compounds were in the form of hexagonal crystals with crystal sizes obtained of 91.14, 78.22 nm, and 51.95 nm respectively by calculation using the Debye Scherrer equation (1):

$$D = \frac{K \cdot \lambda}{\beta \cdot \cos\theta} \quad (1)$$

where D is the average of crystal size, K is the shape factor (0.9), λ is the X-ray wavelength (0.15406 nm), β is the line broadening at full width at half maximum (FWHM = 0.02783) on the 2θ scale in radians and θ is the Bragg angle of the peak in degrees.

The diffractogram shows that all of the compounds produced were hexagonal crystals. The values for "a" and "c" represent the lattice parameters of the hexagonal unit cell. The lattice parameters are different for each sample, with C600 having a = 9.72 Å and c = 6.89 Å, C700 having a = 9.81 Å and c = 6.87 Å, and C800 having a = 9.29 Å and c = 6.81 Å. The carbonization temperature does not affect the crystal structure of the activated carbon. This is because the crystalline phase formed has already been crystallized at 500 °C. This means that the crystal structure remains the same even if the temperature is increased beyond 500 °C. However, as mentioned in the previous paragraph, the carbonization temperature can affect the crystalline quality of activated carbon, with increasing temperature leading to a decrease in crystalline quality beyond a certain limit [21].

3.2 Scanning Electron Microscope (SEM)

The effect of carbonization temperature on the morphological structure of the activated carbon produced was investigated by SEM analysis of samples C600, C700, and C800. Fig. 3 (a, b) displays the SEM image of sample C600 with magnification of 1000 and 2500 times, revealing a lumpy morphology with a relatively rough and solid surface. However, the surface has cracks or breaks that form narrow gaps between them, and impurities attached to the surface associated with calcium elements. The cracks provide an advantage in increasing the surface area of the active surface, thus increasing porosity. ImageJ calculations show a pore/gap size of 1-2 μm, placing it in the macroporous category. High carbonization temperatures favor the formation of well-ordered and penetrable pore channels [22]. while extra high temperatures may plug the pore-mouth, distort the pore-channels, and destroy the pore-structure of biomorphic porous carbon [23]. Carbonization temperature significantly affects the pore structure of activated carbon and is linked to increased density of activated carbon, where the volume of carbon deposits increases with higher carbonization temperatures [24].

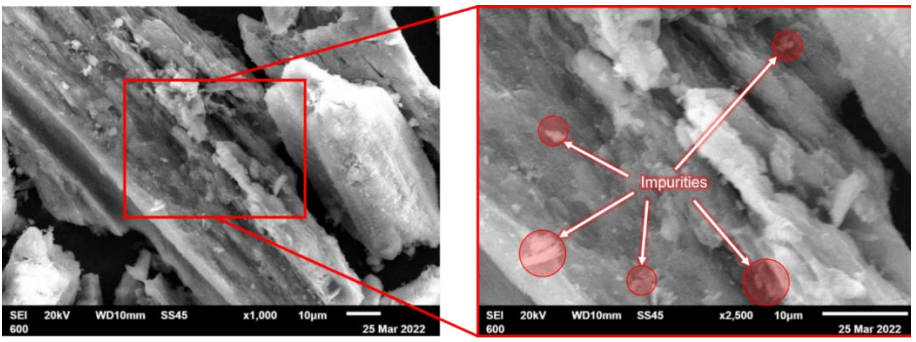

(a) (b)

Fig. 3. SEM image of C600 sample with magnification of 1000 times (a) and 2500 times (b).

Activated carbon is a widely used adsorbent material in various applications, including water treatment, air purification, and gas separation [25]. Its efficiency as an adsorbent depends on the pore structure, which is influenced by the carbonization temperature during its production [26]. Therefore, understanding the effect of carbonization temperature on the pore structure of activated carbon is crucial for optimizing its performance. The results from SEM analysis and ImageJ calculations in this study provide valuable insights into the pore structure of activated carbon produced at different carbonization temperatures. The findings indicate that the morphology of activated carbon is strongly dependent on the carbonization temperature, which affects the pore size, surface area, and pore connectivity. This knowledge can be used to tailor the production process of activated carbon to achieve the desired pore structure and optimize its performance in various applications.

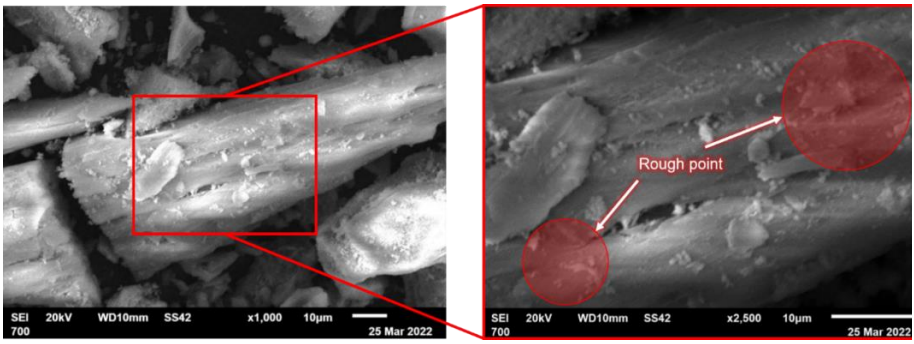

(a) (b)

Fig. 4. SEM image of C700 sample with magnification of 1000 times (a) and 2500 times (b).

Fig. 4 (a, b) depicts the SEM image of sample C700 at 1000 and 2500 times magnification, respectively. Increasing the carbonization temperature of activated carbon results in a change in the surface morphological structure formed in the C700 sample. This change is evident in the level of surface roughness, with a reduction in the size of gaps or cracks on the active surface of the chunks. As the volume of narrow spaces in the gap decreases, density increases. The increase in carbonization temperature from 600 to 700 °C leads to a reduction in pore size, as values of 700-800 nm are obtained through measurements, which still belong to the macroporous category. However, measuring the grain size of activated carbon yields a size of 30-40 μm. While adding temperature can speed up the reaction, excessively high temperatures above 700 °C may result in the formation of ash that can close the pore. Increasing carbonization temperatures release more volatiles and form more macroporous, leading to a decrease in yield and a decrease in the size of the carbon grains. Fig. 5 (a, b) also shows the SEM image of sample C800 at 1000 and 2500 times magnification, where a hollow and porous structure is formed on the side of the surface of activated carbon granules. Additionally, several roughness points were identified on each side of the surface, which can be attributed to the effect of carbonization temperature contributing to the agglomeration of carbon elements.

The reduction in pore size with increasing carbonization temperature can have a significant impact on the performance of activated carbon in various applications. For instance, the pore size distribution of activated carbon is crucial for adsorption processes, where smaller pores can selectively adsorb smaller molecules, while larger pores can adsorb larger molecules [27]. In addition to pore size, the surface area and porosity of activated carbon are also important factors that affect its performance. Higher surface area and porosity lead to increased adsorption capacity and improved efficiency. Therefore, optimizing the carbonization temperature is necessary to achieve the desired pore size, surface area, and porosity, depending on the intended application [28]. Furthermore, the SEM images and analysis provide valuable information for understanding the effect of carbonization temperature on the morphological structure of activated carbon, which can help in designing and improving the production process of activated carbon.

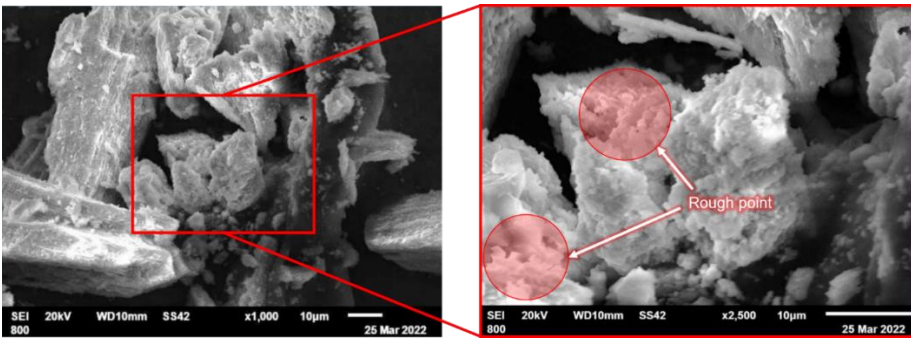

(a) (b)

Fig. 5. SEM image of C600 sample with magnification of 1000 times (a) and 2500 times (b)

4 Conclusion

The carbon samples synthesized from tuna bones exhibited an amorphous structure with crystalline peaks characteristic of the hydroxyapatite crystalline phase. The carbonization temperature of tuna bones did not affect the crystal structure of the activated carbon since the crystalline phase had already formed at 500 °C. However, increasing the carbonization temperature from 600 to 700 °C resulted in a decrease in pore size. Although increasing the temperature can accelerate the reaction, excessively high temperatures, such as those above 700 °C, can lead to the formation of ash, which can clog the pores. Higher carbonization temperatures result in the release of more volatiles and the formation of more macropores, leading to a decrease in yield and a reduction in the size of carbon grains. These findings are consistent with the SEM image of sample C800 in Figure 5 (a, b), which reveals the presence of a hollow and porous structure on the surface of activated carbon granules, with several roughness points on each side that can be attributed to the agglomeration of carbon elements due to the effect of carbonization temperature. Future research could explore the potential applications of tuna bone-derived activated carbon in various fields, such as wastewater treatment, gas purification, and energy storage. Further studies could investigate the specific properties of the carbon samples, such as their adsorption capacity, pore size distribution, and surface area, and compare them with those of other commercially available activated carbons.

Acknowledgments. The authors express their gratitude for the scientific and technical support, as well as the access to facilities provided by the Basic Laboratory of Universitas Sumatera Utara, Advance Characterization Laboratories of National Research and Innovation Agency, Integrated Laboratory of Universitas Islam Indonesia, and Research Institute for Standardization and Industrial Terrain Medan.

References

1. U. Sittitut, J. Jettanasen, S. Supothina, and R. Rattanakam, "Dissolution Performance of Carbon/Hydroxyapatite Nanocomposite Prepared from Fish Scales," *Inorganics*, vol. 10, no. 12, p. 242, Dec. 2022, doi: 10.3390/inorganics10120242.
2. M. Rianna *et al.*, "Evaluation of Co0.7Ni0.3Fe2O4 nano-particle on structural, morphological, and magnetic properties as a heavy metal adsorbent in Cu, Cr," *Mater. Sci. Energy Technol.*, vol. 6, pp. 77–80, 2023, doi: 10.1016/j.mset.2022.11.011.
3. A. Moreno-Santos *et al.*, "Hydroxyapatite Growth on Activated Carbon Surface for Methylene Blue Adsorption: Effect of Oxidation Time and CaSiO3 Addition on Hydrothermal Incubation," *Appl. Sci.*, vol. 13, no. 1, p. 77, Dec. 2022, doi: 10.3390/app13010077.
4. Y. Long, J. Jiang, J. Hu, X. Hu, Q. Yang, and S. Zhou, "Removal of Pb(II) from aqueous solution by hydroxyapatite/carbon composite: Preparation and adsorption behavior," *Colloids Surfaces A Physicochem. Eng. Asp.*, vol. 577, pp. 471–479, Sep. 2019, doi: 10.1016/j.colsurfa.2019.06.011.
5. F. S. Ritonga, S. Humaidi, and Z. Sitorus, "Synthesis of Carbon from Yellowfin Tuna Fishbone to Remove Iron (Fe) Metal in Well Water from Bandar Setia," *J. Phys. Conf. Ser.*, vol. 2376, no. 1, 2022, doi: 10.1088/1742-6596/2376/1/012001.
6. M. M. Ghobashy, N. M. El-Sawy, and A. S. Kodous, "Nanocomposite of cosubstituted carbonated hydroxyapatite fabricated inside Poly(sodium hyaluronate-acrylamide) hydrogel template prepared by gamma radiation for osteoblast cell regeneration," *Radiat. Phys. Chem.*, vol. 183, p. 109408, Jun. 2021, doi: 10.1016/j.radphyschem.2021.109408.
7. Y. Xing *et al.*, "Separation of unburned carbon from coal fly ash: A review," *Powder Technol.*, vol. 353, pp. 372–384, Jul. 2019, doi: 10.1016/j.powtec.2019.05.037.
8. Y. Yin, Q. Liu, J. Wang, and Y. Zhao, "Recent insights in synthesis and energy storage applications of porous carbon derived from biomass waste: A review," *Int. J. Hydrogen Energy*, vol. 47, no. 93, pp. 39338–39363, Dec. 2022, doi: 10.1016/j.ijhydene.2022.09.121.
9. K. MacDermid-Watts, R. Pradhan, and A. Dutta, "Catalytic Hydrothermal Carbonization Treatment of Biomass for Enhanced Activated Carbon: A Review," *Waste and Biomass Valorization*, vol. 12, no. 5, pp. 2171–2186, May 2021, doi: 10.1007/s12649-020-01134-x.
10. C. Guclu, K. Alper, M. Erdem, K. Tekin, and S. Karagoz, "Activated carbons from co-carbonization of waste truck tires and spent tea leaves," *Sustain. Chem. Pharm.*, vol. 21, p. 100410, Jun. 2021, doi: 10.1016/j.scp.2021.100410.
11. K. H. Vardhan, P. S. Kumar, and R. C. Panda, "A review on heavy metal pollution, toxicity and remedial measures: Current trends and future perspectives," *J. Mol. Liq.*, vol. 290, p. 111197, Sep. 2019, doi: 10.1016/j.molliq.2019.111197.
12. T. Varadavenkatesan, R. Vinayagam, S. Pai, B. Kathirvel, A. Pugazhendhi, and R. Selvaraj, "Synthesis, biological and environmental applications of hydroxyapatite and its composites with organic and inorganic coatings," *Prog. Org. Coatings*, vol. 151, p. 106056, Feb. 2021, doi: 10.1016/j.porgcoat.2020.106056.
13. N. A. S. Mohd Pu'ad, P. Koshy, H. Z. Abdullah, M. I. Idris, and T. C. Lee, "Syntheses of hydroxyapatite from natural sources," *Heliyon*, vol. 5, no. 5, p. e01588, May 2019, doi: 10.1016/j.heliyon.2019.e01588.
14. S.-Y. Peng, Y.-W. Lin, W.-H. Lee, Y.-Y. Lin, M.-J. Hung, and K.-L. Lin, "Removal of Cu2+ from wastewater using eco-hydroxyapatite synthesized from marble sludge," *Mater. Chem. Phys.*, vol. 293, p. 126854, Jan. 2023, doi: 10.1016/j.matchemphys.2022.126854.

15. S. Steiner, B. Lothenbach, T. Proske, A. Borgschulte, and F. Winnefeld, “Effect of relative humidity on the carbonation rate of portlandite, calcium silicate hydrates and ettringite,” *Cem. Concr. Res.*, vol. 135, p. 106116, Sep. 2020, doi: 10.1016/j.cemconres.2020.106116.
16. A. Filous *et al.*, “Movements of juvenile yellowfin tuna (Thunnus albacares) within the coastal FAD network adjacent to the Palau National Marine Sanctuary: Implications for local fisheries development,” *Fish. Res.*, vol. 230, p. 105688, Oct. 2020, doi: 10.1016/j.fishres.2020.105688.
17. H. A. Ganaie, “Threats and Risks of Contamination Load on Different Biota,” in *Bioremediation and Biotechnology, Vol 4*, Cham: Springer International Publishing, 2020, pp. 107–124. doi: 10.1007/978-3-030-48690-7_5.
18. A. Ghosh *et al.*, “Structural and electrochemical properties of babassu coconut mesocarp-generated activated carbon and few-layer graphene,” *Carbon N. Y.*, vol. 145, pp. 175–186, Apr. 2019, doi: 10.1016/j.carbon.2018.12.114.
19. G. Zhang, B. Lei, S. Chen, H. Xie, and G. Zhou, “Activated carbon adsorbents with micro-mesoporous structure derived from waste biomass by stepwise activation for toluene removal from air,” *J. Environ. Chem. Eng.*, vol. 9, no. 4, p. 105387, Aug. 2021, doi: 10.1016/j.jece.2021.105387.
20. X. Zhao *et al.*, “Preparation of carbon fiber/Mg-doped nano-hydroxyapatite composites under low temperature by pressureless sintering,” *Ceram. Int.*, vol. 48, no. 1, pp. 674–683, Jan. 2022, doi: 10.1016/j.ceramint.2021.09.147.
21. Q. Pu *et al.*, “Systematic study of dynamic CO2 adsorption on activated carbons derived from different biomass,” *J. Alloys Compd.*, vol. 887, p. 161406, Dec. 2021, doi: 10.1016/j.jallcom.2021.161406.
22. Z. Zhang, N. Sun, and W. Wei, “Facile and controllable synthesis of ordered mesoporous carbons with tunable single-crystal morphology for CO2 capture,” *Carbon N. Y.*, vol. 161, pp. 629–638, May 2020, doi: 10.1016/j.carbon.2020.02.009.
23. M. S. Rana, F. S. AlHumaidan, and R. Navvamani, “Synthesis of large pore carbon-alumina supported catalysts for hydrodemetallization,” *Catal. Today*, vol. 353, pp. 204–212, Aug. 2020, doi: 10.1016/j.cattod.2019.07.009.
24. J. Gopalan, A. Buthiyappan, and A. A. Abdul Raman, “Insight into metal-impregnated biomass based activated carbon for enhanced carbon dioxide adsorption: A review,” *J. Ind. Eng. Chem.*, vol. 113, pp. 72–95, Sep. 2022, doi: 10.1016/j.jiec.2022.06.026.
25. M. Nasrollahzadeh, M. Sajjadi, S. Iravani, and R. S. Varma, “Carbon-based sustainable nanomaterials for water treatment: State-of-art and future perspectives,” *Chemosphere*, vol. 263, p. 128005, Jan. 2021, doi: 10.1016/j.chemosphere.2020.128005.
26. M. Sweetman *et al.*, “Activated Carbon, Carbon Nanotubes and Graphene: Materials and Composites for Advanced Water Purification,” *C*, vol. 3, no. 4, p. 18, Jun. 2017, doi: 10.3390/c3020018.
27. Z. Li, Y. Li, and J. Zhu, “Straw-Based Activated Carbon: Optimization of the Preparation Procedure and Performance of Volatile Organic Compounds Adsorption,” *Materials (Basel).*, vol. 14, no. 12, p. 3284, Jun. 2021, doi: 10.3390/ma14123284.
28. S. Chen *et al.*, “Preparation of porous carbon-based material from corn straw via mixed alkali and its application for removal of dye,” *Colloids Surfaces A Physicochem. Eng. Asp.*, vol. 568, pp. 173–183, May 2019, doi: 10.1016/j.colsurfa.2019.02.008.